

**Effect of metal coordination on the interaction of  
substituted phenanthroline and pyridine ligands with  
quadruplex DNA**

Julie E. Reed,<sup>1,2,3</sup> Andrew J. P. White,<sup>1</sup> Stephen Neidle,<sup>2</sup> Ramón Vilar\*<sup>1,2</sup>

<sup>1</sup>*Department of Chemistry, Imperial College London, South*

*Kensington, London SW7 2AZ, UK*

<sup>2</sup>*CRUK Biomolecular Structure Group, The School of Pharmacy*

*University of London, London WC1N 1AX, UK*

<sup>3</sup>*Institute of Chemical Research of Catalonia (ICIQ), Avgda. Països*

*Catalans 16, 43007 Tarragona, SPAIN*

**Corresponding author:**

Dr. Ramon Vilar  
Department of Chemistry  
Imperial College London  
London SW7 2AZ  
UK

Email: r.vilar@imperial.ac.uk  
Telephone: +44(0)2075941967  
Fax: +44(0)2075941139

## Supplementary Information

### 1. X-ray crystallography.

The N–H and O–H protons in the structures of **L**<sup>1</sup> and **L**<sup>6</sup> were found from  $\Delta F$  maps and refined subject to an X–H distance constraint (0.90 Å). The N–H and O–H protons in **2** could not be located and so were not included. The O–H protons in **6** could not be located from  $\Delta F$  maps and so were added in idealised positions and allowed to rotate about the associated C–O bonds (HFIX 147). The included solvent in **2** is highly disordered; in particular three orientations were identified for the dmso solvent. However, the indications are that this is merely a small subset of the orientations present for this molecule and so the hydrogen bonding interaction to this area need to be treated with caution.

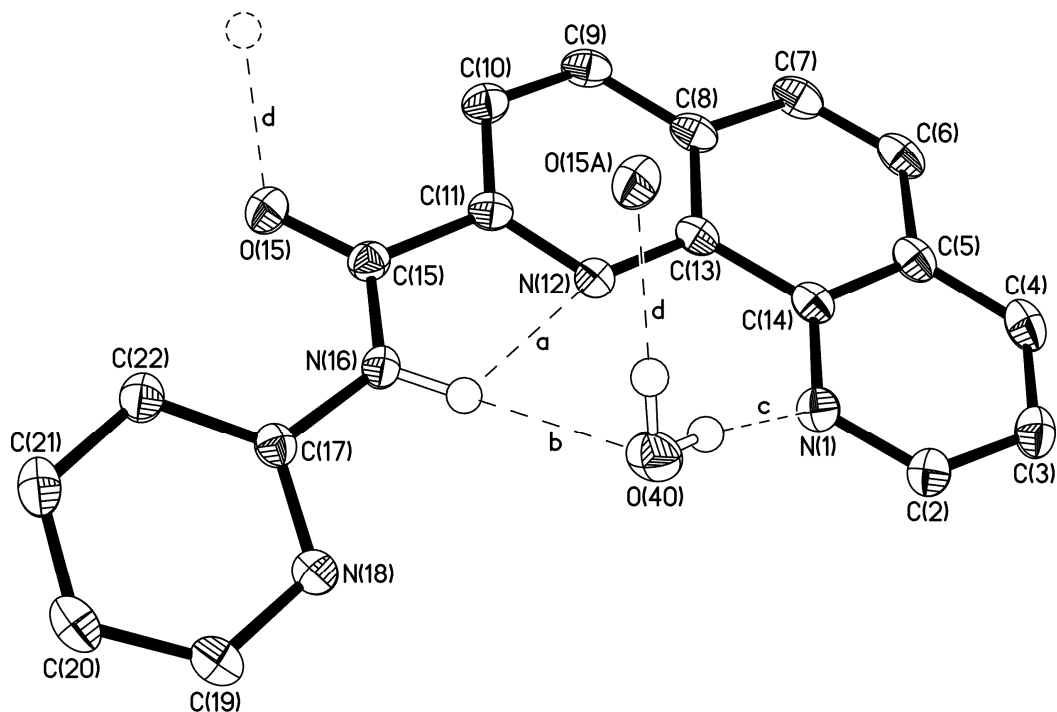


**Fig. S1** The molecular structure of **L**<sup>1</sup> (50% probability ellipsoids).

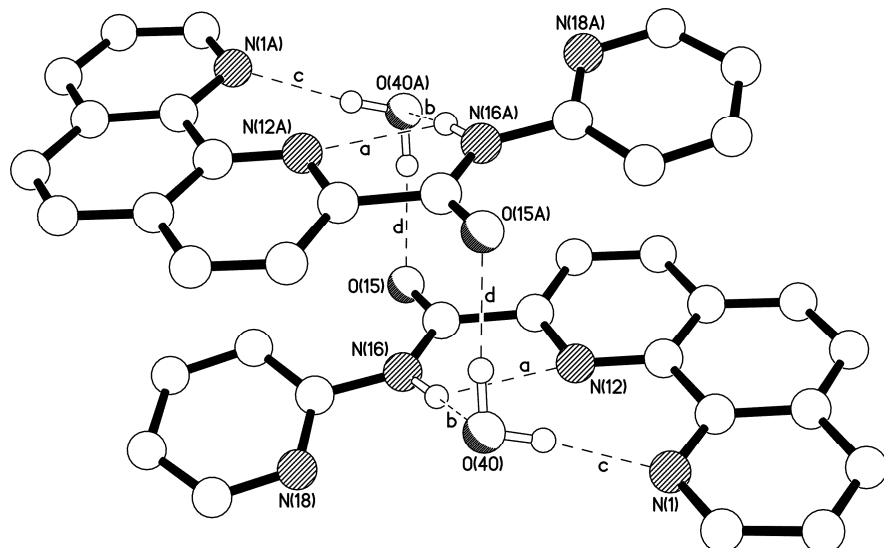


**Fig. S2** One of the hydrogen-bonded dimers pairs present in the structure of  $\mathbf{L}^1$ .

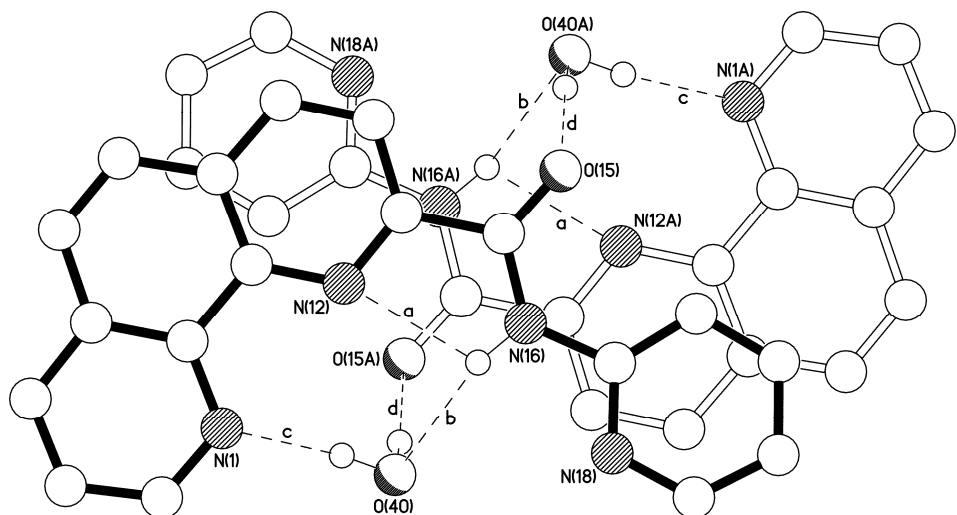
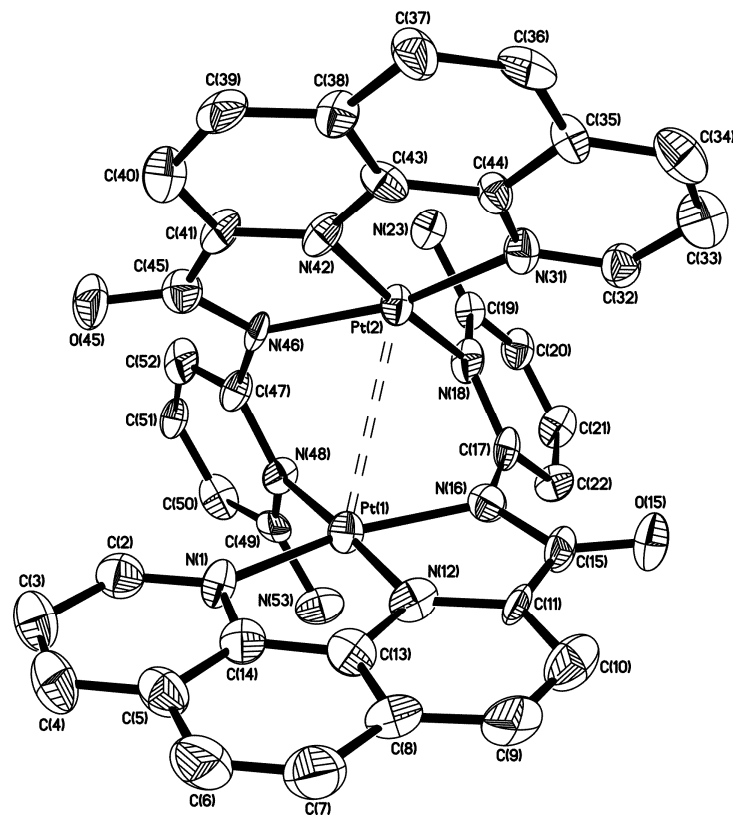
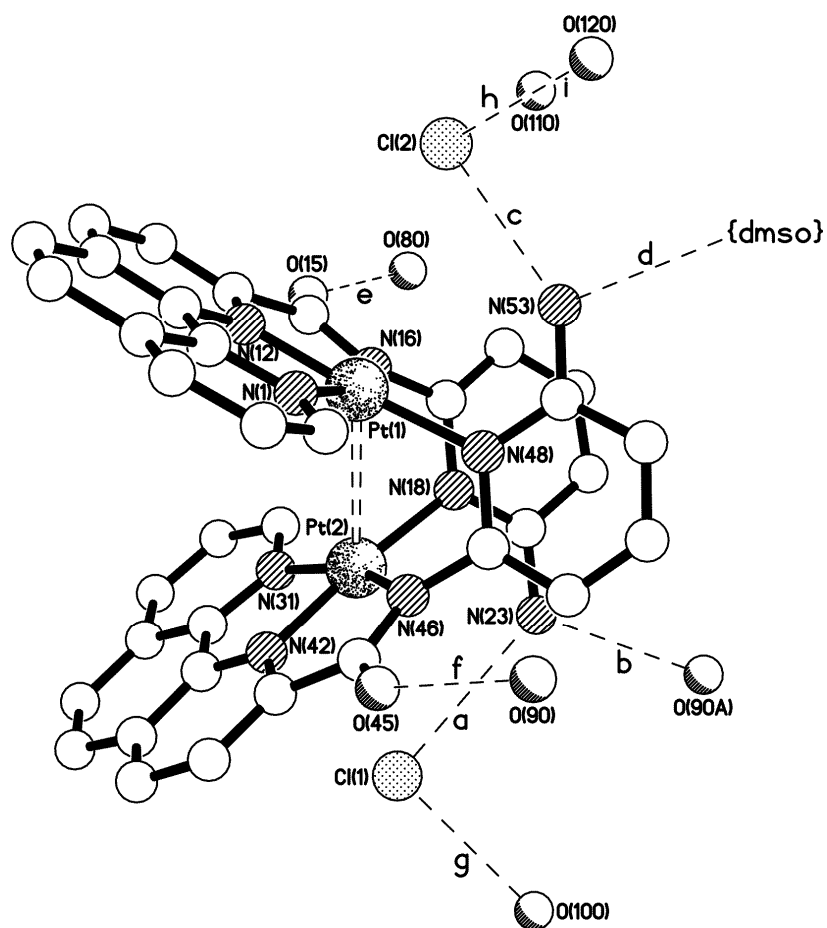


Fig. S3

**Fig. S3** One of the hydrogen-bonded dimers pairs present in the structure of  $\mathbf{L}^1$  viewed in parallel projection perpendicular to the mean plane of the molecule, showing the overlap between the N(12) aromatic ring in one molecule and the N(18) aromatic ring in its centrosymmetrically related counterpart. The centroid...centroid and mean interplanar separations for these  $C_5N$  rings are 3.74 and 3.43 Å respectively, the two rings being inclined by *ca.* 11°.



**Fig. S4** The molecular structure of the dication in **2** viewed down the molecular  $C_2$  axis. (50% probability ellipsoids).



**Fig. S5** The hydrogen bonding interactions involving the cation and anions in the structure of **2**. The hydrogen bonding geometries [X···Y Å] are **ab**) 2.885(13); **c**) 3.374(11); **d**) 2.73(3); **e**) 2.798(12); **f**) 2.877(11); **g**) 3.164(10); **h**) 3.193(15); **i**) 3.25(3). The dmso solvent molecule is highly disordered and so the contact distance for interaction **d** should be treated with caution. However, it is clear that there is some kind of interaction between the N(53) NH<sub>2</sub> unit and the area occupied by the dmso solvent.

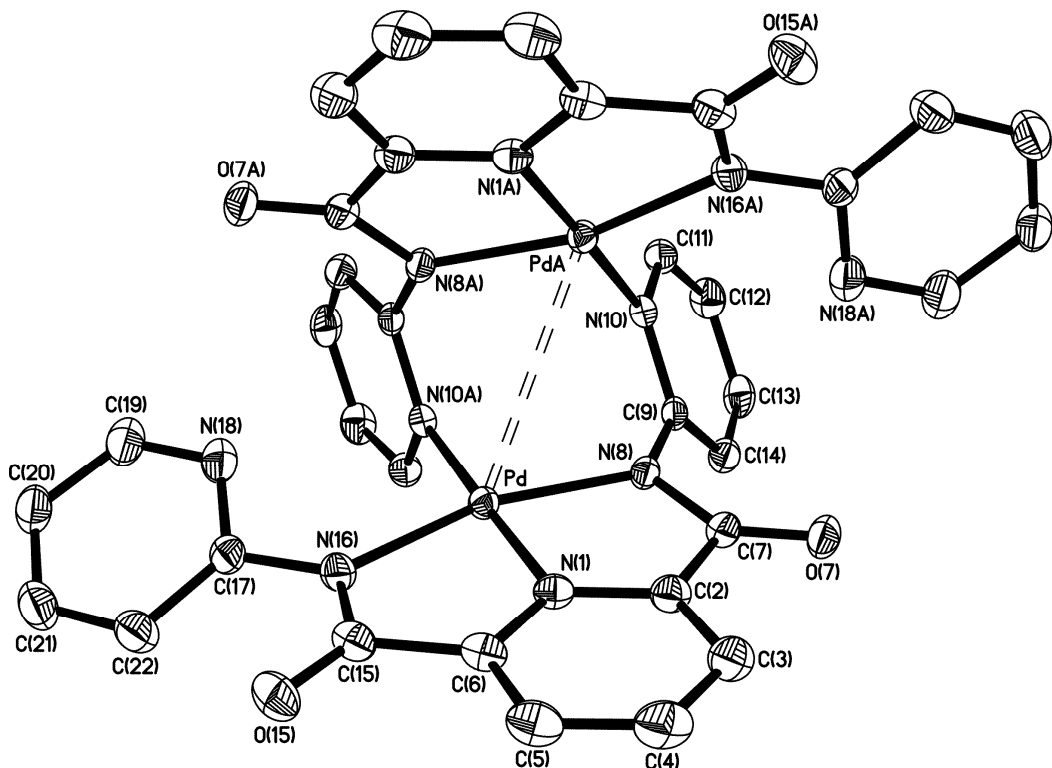


**Fig. S6** The molecular structure of the  $C_2$ -symmetric complex **6** viewed down the  $C_2$  axis (50% probability ellipsoids).

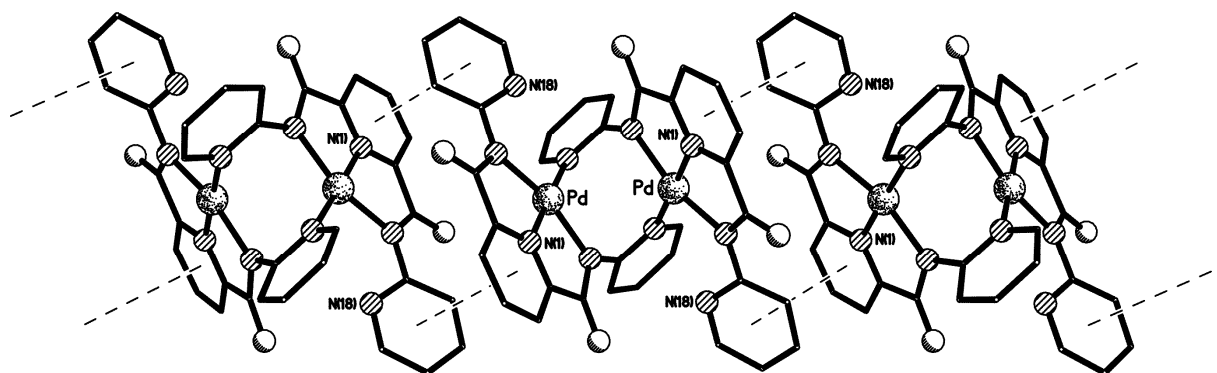


**Fig. S7** Part of one of the extended chains of  $\pi$ - $\pi$  stacked molecules along the  $a$  axis direction present in the crystals of **6** showing the stacking between the N(1) ring in one molecule and the N(18) ring in its centrosymmetrically related counterpart, and *vice versa*. The centroid···centroid and mean interplanar separations are *ca.* 3.81 and 3.65 Å respectively, the two rings being inclined by *ca.* 28°.

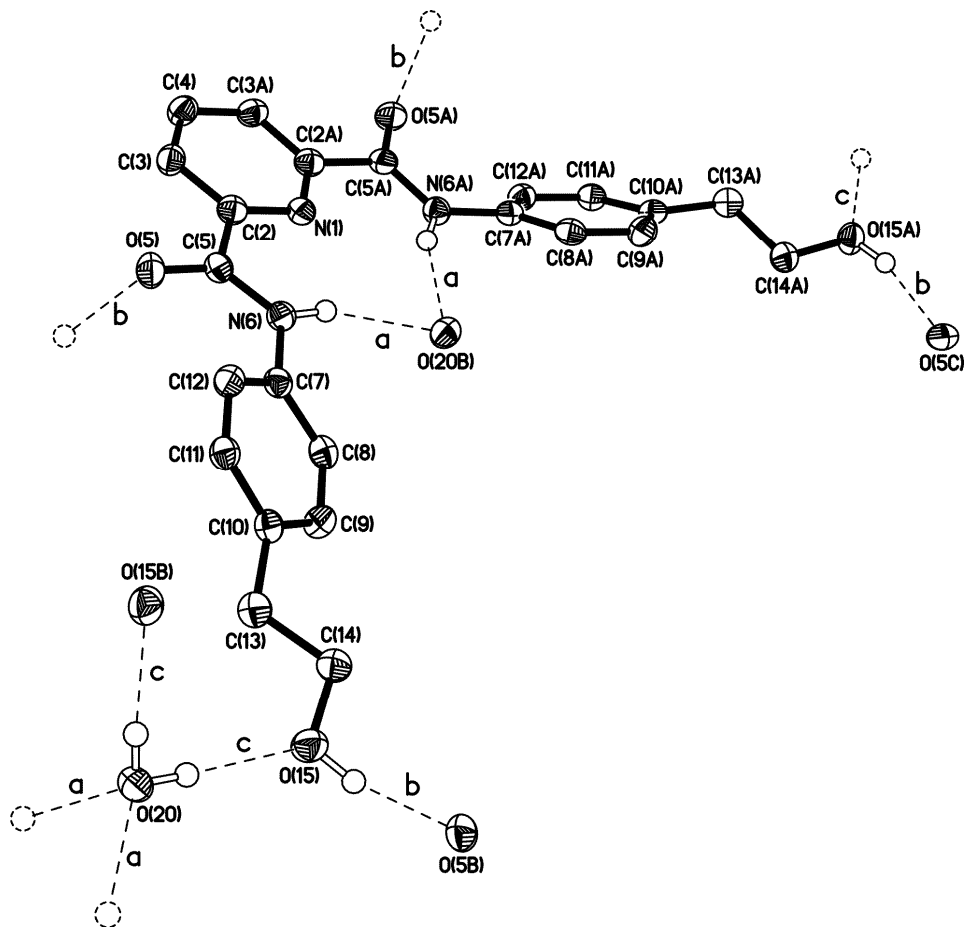


**Fig. S8** The molecular structure of  $\mathbf{L}^6$  (50% probability ellipsoids).

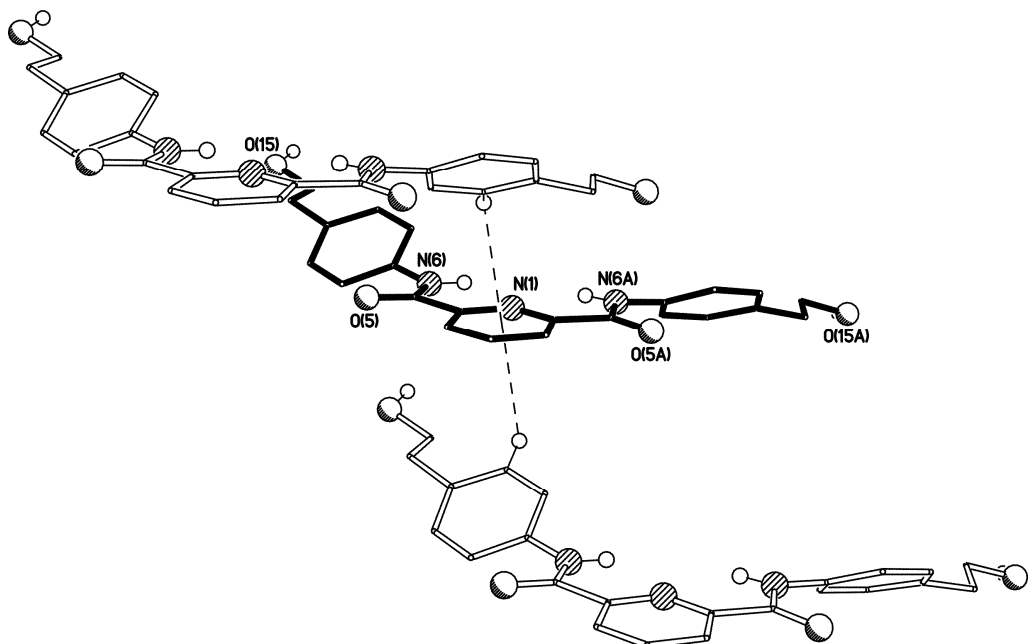


**Fig. S9** Part of the packing in the structure of  $\mathbf{L}^6$  showing the C–H $\cdots$  $\pi$  contacts to the N(1) pyridyl ring.

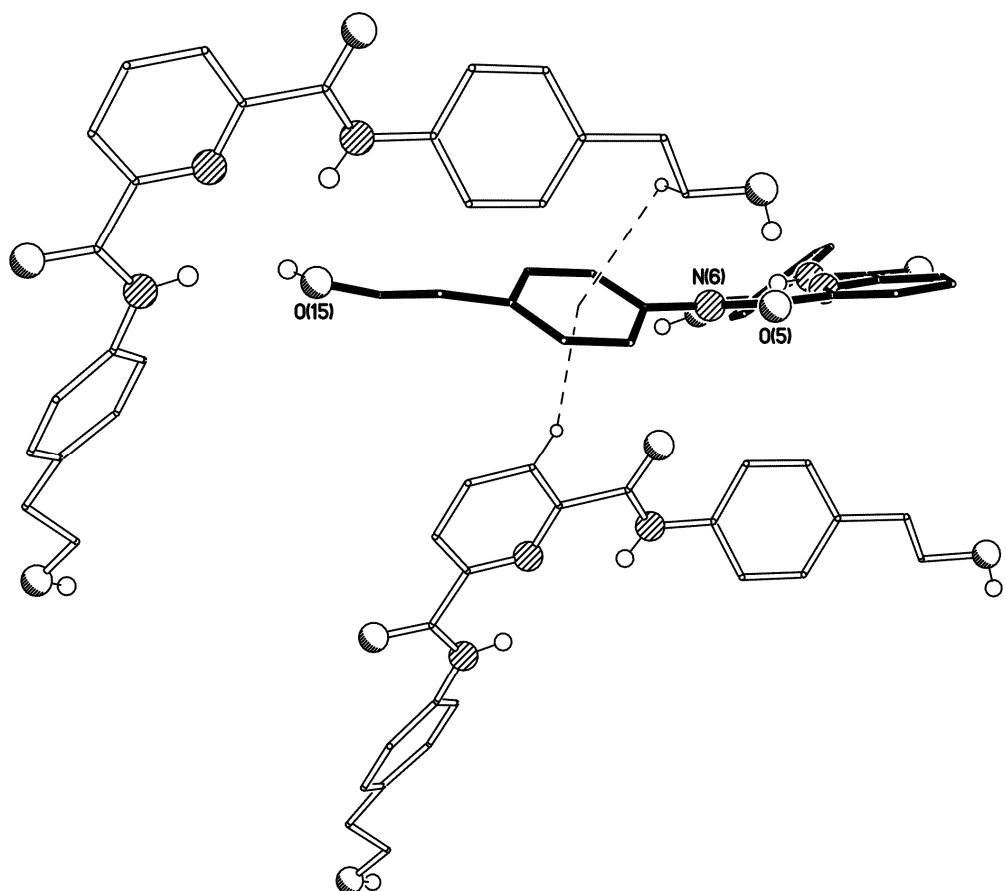


**Fig. S10** Part of the packing in the structure of  $\mathbf{L}^6$  showing the C–H $\cdots$  $\pi$  contacts to the N(6)-bound phenyl ring.

## 2. FRET studies

### 2.1 Quadruplex DNA melting curves determined by FRET

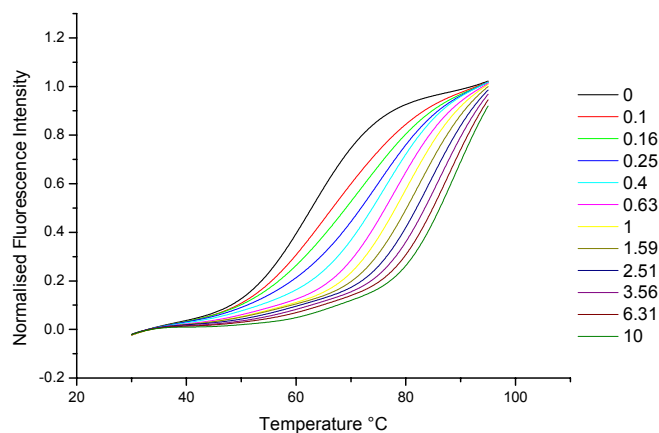


**Fig. S11.** Quadruplex DNA melting curves for different concentrations (values in plot given in  $\mu\text{M}$ ) of complex **1**

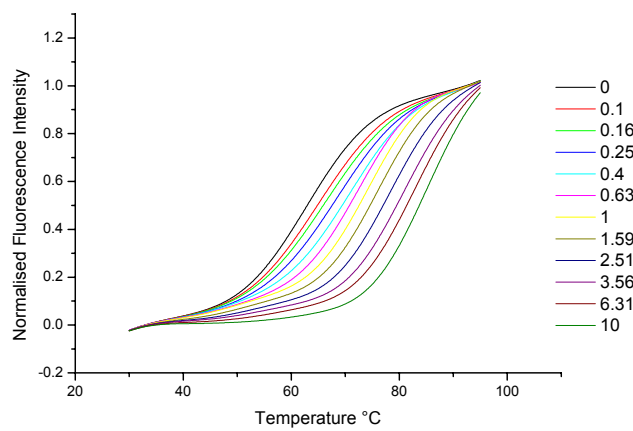


**Fig. S12.** Quadruplex DNA melting curves for different concentrations (values in plot given in  $\mu\text{M}$ ) of complex **2**

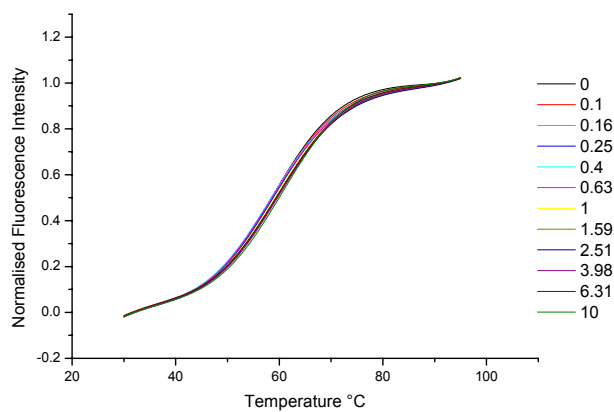


**Fig. S13.** Quadruplex DNA melting curves for different concentrations (values in plot given in  $\mu\text{M}$ ) of **L3**

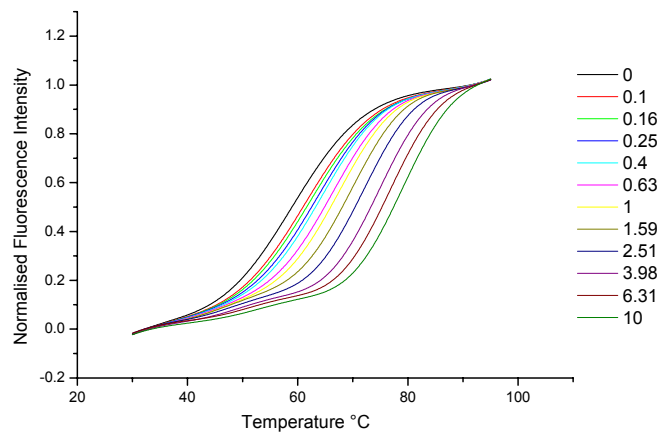


**Fig. S14.** Quadruplex DNA melting curves for different concentrations (values in plot given in  $\mu\text{M}$ ) of **L4**

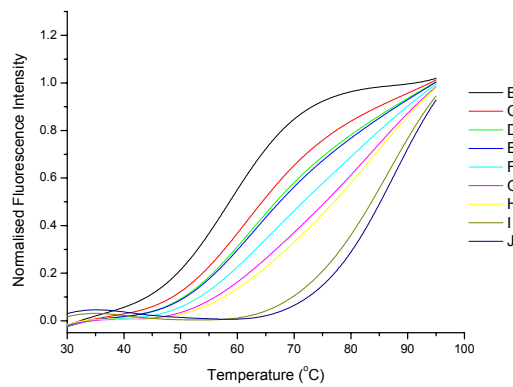


**Fig. S15.** Quadruplex DNA melting curves for different concentrations (values in plot given in  $\mu\text{M}$ ) of complex **4**

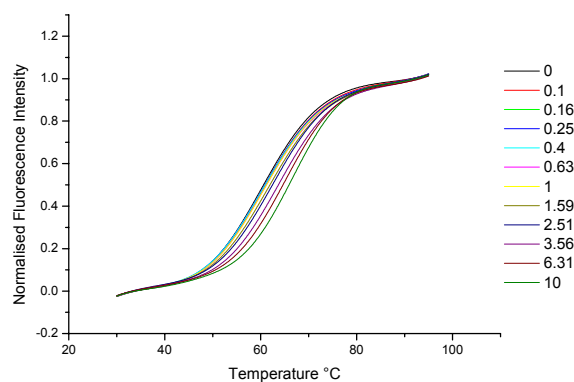


**Fig. S16.** Quadruplex DNA melting curves for different concentrations (values in plot given in  $\mu\text{M}$ ) of **L6**

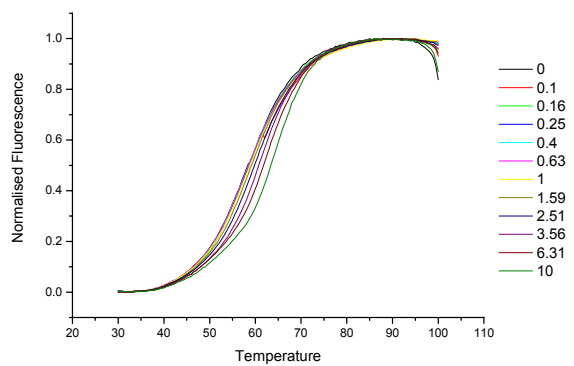


**Fig. S17.** Quadruplex DNA melting curves for different concentrations (values in plot given in  $\mu\text{M}$ ) of **L7**

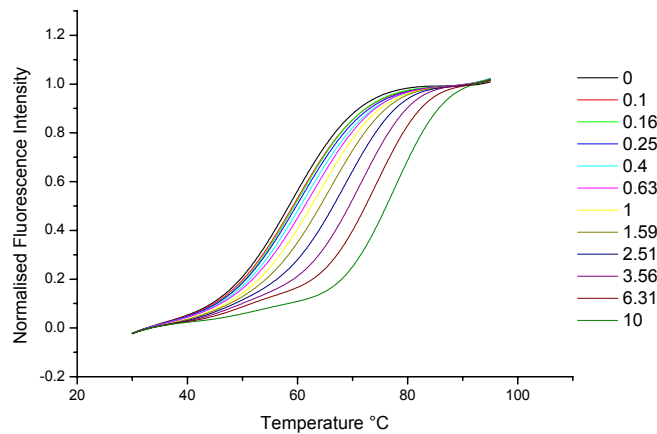


**Fig. S18.** Quadruplex DNA melting curves for different concentrations (values in plot given in  $\mu\text{M}$ ) of **L8**

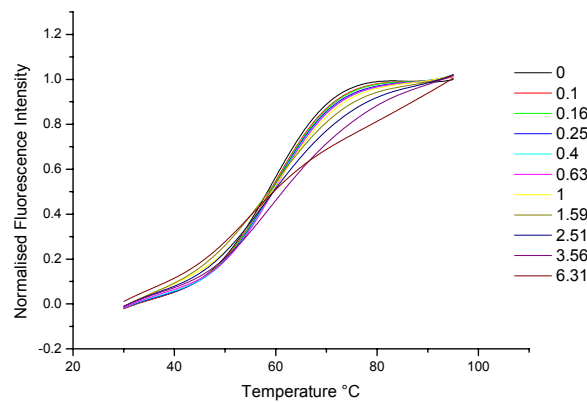


**Fig. S19.** Quadruplex DNA melting curves for different concentrations (values in plot given in  $\mu\text{M}$ ) of complex **7**

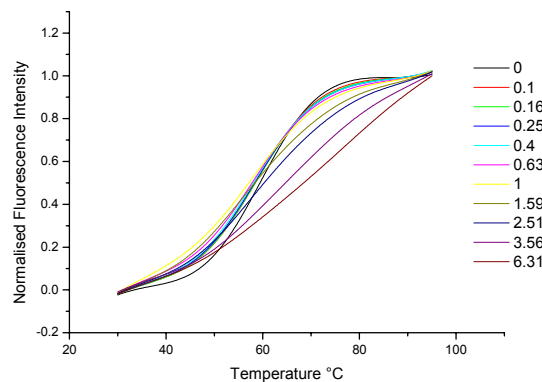


**Fig. S20.** Quadruplex DNA melting curves for different concentrations (values in plot given in  $\mu\text{M}$ ) of complex **8**

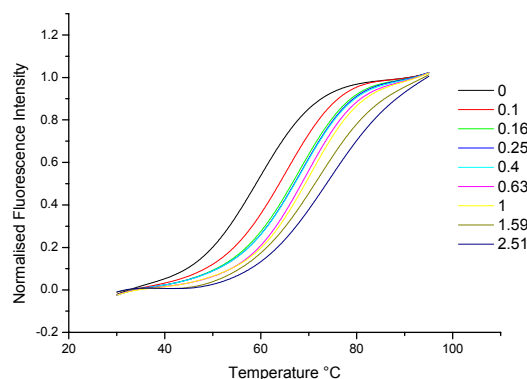


**Fig. S21.** Quadruplex DNA melting curves for different concentrations (values in plot given in  $\mu\text{M}$ ) of complex **9**

## 2.2 Quadruplex DNA melting curves determined by FRET

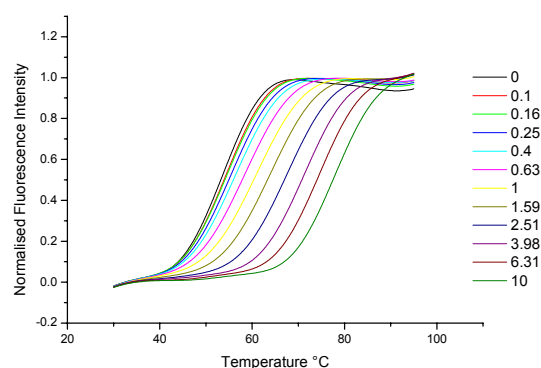


**Fig. S22.** Duplex DNA melting curves for different concentrations (values in plot given in  $\mu\text{M}$ ) of complex **1**

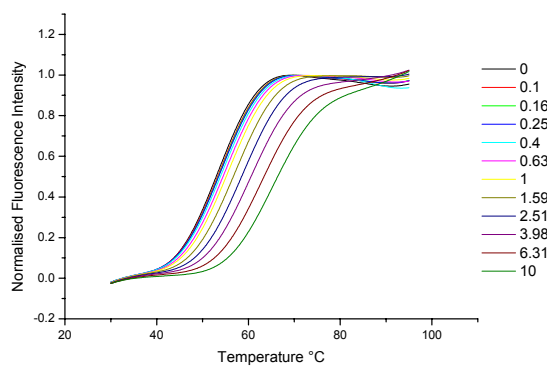


**Fig. S23.** Duplex DNA melting curves for different concentrations (values in plot given in  $\mu\text{M}$ ) of complex **2**

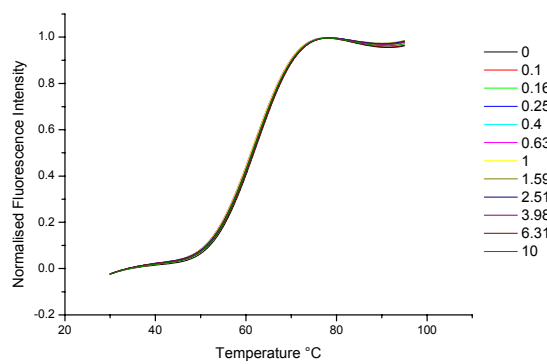


**Fig. S24.** Duplex DNA melting curves for different concentrations (values in plot given in  $\mu\text{M}$ ) of **L3**

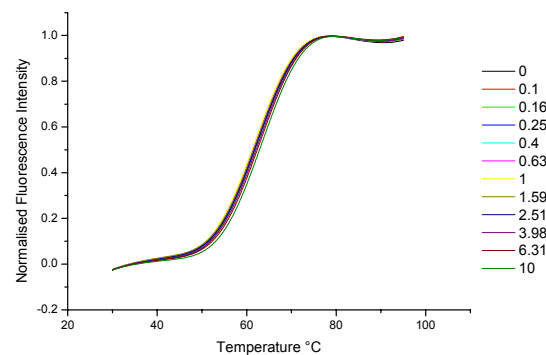


**Fig. S25.** Duplex DNA melting curves for different concentrations (values in plot given in  $\mu\text{M}$ ) of **L4**

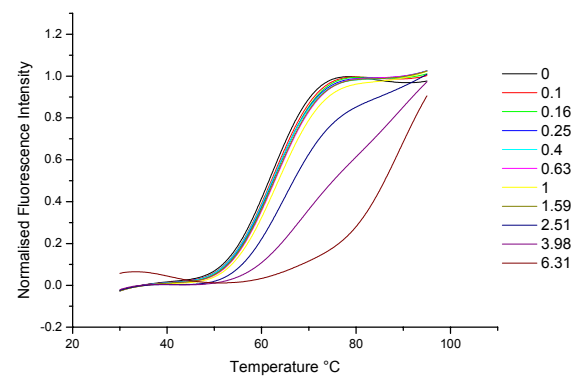


**Fig. S26.** Duplex DNA melting curves for different concentrations (values in plot given in  $\mu\text{M}$ ) of complex **4**

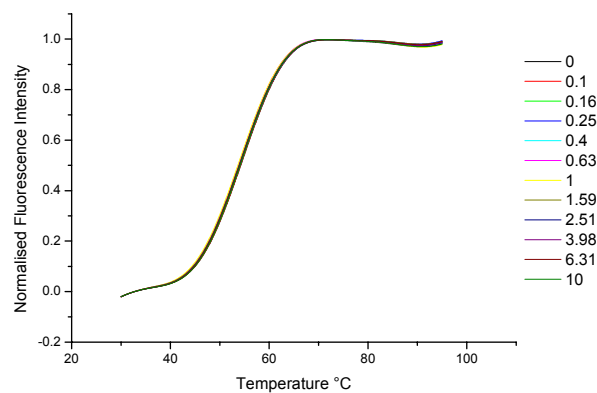


**Fig. S27.** Duplex DNA melting curves for different concentrations (values in plot given in  $\mu\text{M}$ ) of **L6**

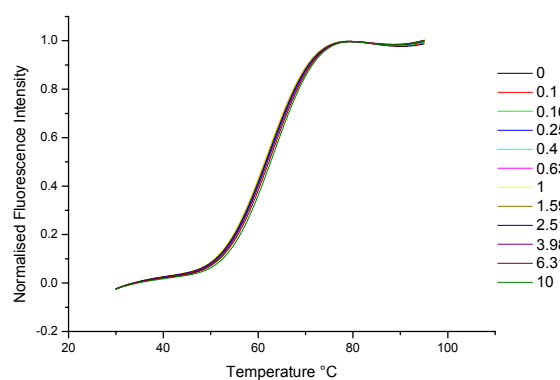


**Fig. S28.** Duplex DNA melting curves for different concentrations (values in plot given in  $\mu\text{M}$ ) of **L8**

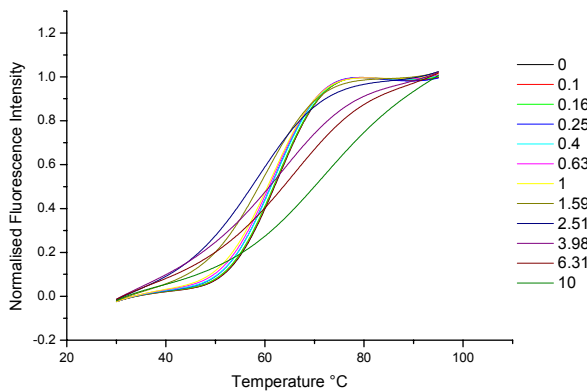


**Fig. S29.** Duplex DNA melting curves for different concentrations (values in plot given in  $\mu\text{M}$ ) of complex **7**

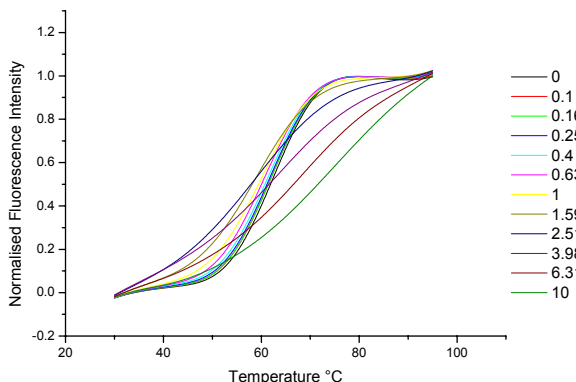


**Fig. S30.** Duplex DNA melting curves for different concentrations (values in plot given in  $\mu\text{M}$ ) of complex **8**

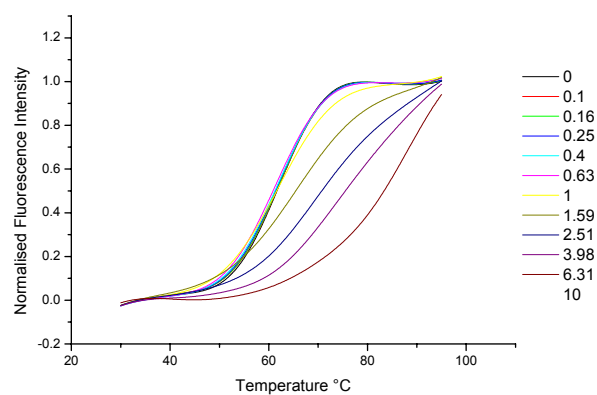


**Fig. S31.** Duplex DNA melting curves for different concentrations (values in plot given in  $\mu\text{M}$ ) of complex **9**